Boundary Value Problems in Orthotropic Micropolar Thermoelastic Medium with One Relaxation Time

§Rajneesh Kumar and †Rajani Rani Gupta

Department of Mathematics, Kurukshetra University
KURUKSHETRA, HARYANA, INDIA
E-mail: §rajneesh_kuk@rediffmail.com, †rajani_gupta_83@yahoomail.com

ABSTRACT

The present investigation is concerned with boundary value problems in orthotropic micropolar thermoelastic medium with one relaxation time as a result of inclined load. The inclined load is assumed to be a linear combination of a normal load and a tangential load. Laplace and Fourier's transform are used to solve the problem. Various types of sources have been taken to illustrate the utility of the approach. The transformed components of Normal force stress, Tangential force stress, Tangential couple stress and Temperature distribution are inverted using numerical inversion techniques. The effect of anisotropy has been shown on the resulting expressions graphically.

Key Words: Orthotropic, Micropolar, Couple stress, Fourier transform, Laplace transform, Microrotation.

1. INTRODUCTION

Micropolar elasticity theory introduced by Eringen /4/ incorporates the local deformation and rotations of the material points of a body. The theory provides a model that can support body and surface couples and display a high frequency optical branch of the wave spectrum. For engineering applications, it can model composites with rigid chopped fibers, elastic solids with rigid granular inclusions, and other industrial materials such as liquid crystals /4, 6, 9/. Several investigations reveal an interesting phenomenon that characterizes the micropolar theory and some of its generalizations are contained in /7,8,12/ .

The linear theory of micropolar thermoelasticity was developed by extending the theory of micropolar continua to include thermal effects by Nowacki /13/ and Eringen /5/. Tauchert *et al* /26/ also derived the basic equations of linear theory of micropolar thermoelasticity. Dost and Tabarrok /3/ presented micropolar generalized thermo-elasticity by using the Green -Lindsay theory. One can refer to Dhaliwal and Singh /25/

for a review on micropolar thermoelasticity. Chandrasekhariah /1/ formulated a theory of micropolar thermoelasticity which includes heat-flux among the constitutive variables.

The dynamic response functions of elastically anisotropic solids are of interest in many fields including crystal acoustics, solid-state physics, non-destructive testing , material characterization, seismology, applied mechanics and mathematics. In recent years the elastodynamic response of anisotropic continuum has received the attention of several researchers.

Iesan /2/ investigated the static theory of anisotropic micropolar elastic solids and proved the positive definiteness of his operator for the first boundary value problem. Kumar *et al.*/14-21/ investigated boundary value problems in an orthotropic micropolar continua and micropolar thermoelastic medium possessing cubic symmetry /22-24/.

The present investigation seeks to determine the components of normal force stress, tangential couple stress and temperature distribution due to concentrated, distributed and moving forces in time domain, frequency domain and steady state due to the inclined load in an orthotropic micropolar thermoelastic medium with one relaxation. The solution is obtained after employing an integral transform technique. The integral transforms are inverted using a numerical method.

2. FORMULATION AND SOLUTION OF THE PROBLEM

We consider an orthotropic micropolar thermoelastic half-space with one relaxation time, having x_2 -axis vertically downwards. Suppose that an inclined load F_0, per unit length, is acting along the interface on the x_3 -axis and its inclination with x_2 -axis is θ.

The basic equations in the dynamic theory of the plain strain of a homogeneous, orthotropic micropolar thermoelastic solid with one relaxation time in absence of body forces, body couples and heat sources can be recalled as:

$$t_{ji,j} = \rho u_i , \tag{1}$$

$$m_{i3,i} + \varepsilon_{ij3} t_{ij} = \rho j \phi_3 , \qquad \text{i=1, 2.} \tag{2}$$

and the heat conduction equation is given by,

$$K_1^* \frac{\partial^2 T}{\partial x_1^2} + K_2^* \frac{\partial^2 T}{\partial x_2^2} = \rho C^* \left(\frac{\partial T}{\partial t} + \tau_0 \frac{\partial^2 T}{\partial t^2}\right) + T_0 \left(\frac{\partial}{\partial t} + \tau_0 \frac{\partial^2}{\partial t^2}\right)\left(\beta_1 \frac{\partial u_1}{\partial x_1} + \beta_2 \frac{\partial u_2}{\partial x_2}\right). \tag{3}$$

The constitutive relations are:

$$\begin{aligned} t_{11} &= A_{11}\varepsilon_{11} + A_{12}\varepsilon_{22} - \beta_1 T , \quad t_{12} = A_{77}\varepsilon_{12} + A_{78}\varepsilon_{21} , \quad m_{13} = B_{66}\phi_3 , \\ t_{22} &= A_{12}\varepsilon_{11} + A_{22}\varepsilon_{22} - \beta_2 T , \quad t_{21} = A_{78}\varepsilon_{12} + A_{88}\varepsilon_{21} , \quad m_{23} = B_{44}\phi_{3,2} , \end{aligned} \tag{4}$$

where

$$\varepsilon_{ij} = u_{j,i} + \varepsilon_{ji3}\phi_3 . \tag{5}$$

Here, the relations between β_i and the coefficients of thermal expansions α_i are

$$\beta_1 = A_{11}\alpha_1 + A_{12}\alpha_2 ,$$
$$\beta_2 = A_{21}\alpha_1 + A_{22}\alpha_2 .$$

In the above equations (1)-(5), we have used the following notations:
t_{ij} Components of the force stress tensor, m_{ij} components of the couple stress tensor, ε_{ij} and components of micropolar strain tensor, u_i components of displacement vector, ϕ_3 component of microrotation vector, ε_{ijk} permutation symbol, τ_0 is the relaxation time, A_{11}, A_{12}, A_{22}, A_{77}, A_{78}, A_{88}, B_{44}, B_{66} are characteristic constants of the material, C^* is the specific heat, K_1^* and K_2^* are the thermal conductivities.

For the two dimensional problem, we take the components of the displacement and microrotation vector in an orthotropic micropolar generalized thermoelastic solid of the form

$$\vec{u} = (u_1, u_2, 0), \qquad \vec{\phi} = (0, 0, \phi_3) . \tag{6}$$

We define the dimensionless variables by the expressions:

$$(x_1', x_2') = \frac{\omega^*}{c_1}(x_1, x_2), \quad (u_1', u_2') = \frac{\rho c_1 \omega^*}{\beta_1 T_0}(u_1, u_2), \quad \phi_3' = \frac{\rho c_1^2}{\beta_1 T_0}\phi_3, \quad t_{ij}' = \frac{t_{ij}}{\beta_1 T_0},$$
$$m'_{23} = \frac{\omega^*}{c_1 \beta_1 T_0} m_{23}, \quad T' = \frac{T}{T_0}, \quad t' = \omega^* t, \quad \tau_0' = \omega^* \tau_0, \quad \omega' = \frac{\omega}{\omega^*}, \tag{7}$$

where

$$\omega^* = \frac{\rho C^* c_1^2}{K_1^*}, \quad c_1^2 = \frac{A_{11}}{\rho} .$$

With the help of equations (4)-(7), equations (1)-(3) take the form (on suppressing the prime):

$$\left(\frac{\partial^2}{\partial x_2^2} + d_1 d_4 \frac{\partial^2}{\partial x_1^2}\right)u_1 + (d_2 + d_3)\frac{\partial^2 u_2}{\partial x_1 \partial x_2} - (d_3 - 1)\frac{\partial \phi_3}{\partial x_2} - d_1 d_4 \frac{\partial T}{\partial x_1} = d_1 d_4 \frac{\partial^2 u_1}{\partial t^2}, \tag{8}$$

$$\frac{(d_2+d_3)}{d_4}\frac{\partial^2 u_1}{\partial x_1 \partial x_2}+\left(\frac{\partial^2}{\partial x_2^2}+\frac{d_5}{d_4}\frac{\partial^2}{\partial x_1^2}\right)u_2-\frac{(d_5-d_3)}{d_4}\frac{\partial \phi_3}{\partial x_1}-\beta d_1\frac{\partial T}{\partial x_2}=d_1\frac{\partial^2 u_2}{\partial t^2}, \tag{9}$$

$$\left(\frac{\partial^2}{\partial x_2^2}+d_6\frac{\partial^2}{\partial x_1^2}-d_7(d_5-2d_3+1)\right)\phi_3+d_7(d_3-1)\frac{\partial u_1}{\partial x_2}+d_7(d_5-d_3)\frac{\partial u_2}{\partial x_1}=d_8\frac{\partial^2 \phi_3}{\partial t^2}, \tag{10}$$

$$\left(\frac{\partial^2}{\partial x_1^2}+\bar{K}\frac{\partial^2}{\partial x_2^2}\right)T=\left(\frac{\partial}{\partial t}+\tau_0\frac{\partial^2}{\partial t^2}\right)T+\varepsilon\left(\frac{\partial}{\partial t}+n_0\tau_0\frac{\partial^2}{\partial t^2}\right)\left(\frac{\partial u_1}{\partial x_1}+\beta\frac{\partial u_2}{\partial x_2}\right), \tag{11}$$

where

$$d_1=\frac{A_{11}}{A_{22}},\quad d_2=\frac{A_{12}}{A_{88}},\quad d_3=\frac{A_{78}}{A_{88}},\quad d_4=\frac{A_{22}}{A_{88}},\quad d_5=\frac{A_{77}}{A_{88}},\quad d_7=\frac{A_{88}c_i^2}{B_{44}\omega^{*2}},\quad d_8=\frac{\rho j c_i^2}{B_{44}},$$

$$K^*=\frac{K_2^*}{K_1^*},\quad \beta^*=\frac{\beta_2}{\beta_1},\quad \varepsilon=\frac{\beta_1^2 T_0}{\rho K_1^* \omega^*}.$$

We define the Laplace and Fourier transforms as follows:

$$\bar{f}(x_1,x_2,p)=\int_0^\infty f(x_1,x_2,t)e^{-pt}dt, \tag{12}$$

$$\bar{f}(\xi,x_2,p)=\int_{-\infty}^{\infty}\bar{f}(x_1,x_2,t)e^{i\xi x}dx_1. \tag{13}$$

3 BOUNDARY CONDITIONS

The boundary conditions on the surface $x_2=0$ are given by

(i) $t_{22}=-P_1\psi_1(x_1)\eta(t)$,
(ii) $t_{21}=-P_2\psi_2(x_1)\eta(t)$,
(iii) $m_{23}=0$,
(iv) T=0, (14)

where P_1 and P_2 are the magnitudes of force and $\psi_1(x_1),\psi_2(x_1)$ are defined later in this paper and $\eta(t)$ take the different values in time domain and frequency domain.

Case I- Concentrated Force

To determine the normal force stress, tangential force stress, tangential couple stress and temperature distribution due to concentrated force described by Dirac delta function

$$\left.\begin{matrix}\psi_1(x_1)\\ \psi_2(x_1)\end{matrix}\right\} = \delta(x_1),$$

which must be used with

$$\left.\begin{matrix}\psi_1(\xi)\\ \psi_2(\xi)\end{matrix}\right\} = 1. \tag{15}$$

Case II- Distributed Force

The solution due to force distributed over a strip of width 2a, applied on the half space is obtained by setting

$$\left.\begin{matrix}\psi_1(x_1)\\ \psi_2(x_1)\end{matrix}\right\} = H(x_1 + a) - H(x_1 - a), \tag{16}$$

in equation (14). Using equation (7) and then applying Fourier transforms defined by equation (13) on equation (16) we obtain,

$$\left.\begin{matrix}\psi_1(x_1)\\ \psi_2(x_1)\end{matrix}\right\} = .2\sin\left(\frac{\xi c_1 a}{\omega^*}\right)/\xi. \tag{17}$$

Case III- Moving Force

The solution due to an impulsive force, moving along the x_1-axis with uniform speed V at $x_2 = 0$ is obtained by setting

$$\left.\begin{matrix}\psi_1(x_1)\eta(t)\\ \psi_2(x_1)\eta(t)\end{matrix}\right\} = \psi(x_1, t) = \delta(x_1 - Vt), \tag{18}$$

in equation (14). Using equation (7) and then applying Laplace and Fourier transform's defined by equation (12) and (13) on the equation (18) we obtain,

$$\left.\begin{matrix}\psi_1(\xi)\bar{\eta}(p)\\ \psi_2(\xi)\bar{\eta}(p)\end{matrix}\right\} = \bar{\psi}(\xi, p) = \frac{1}{p - i\xi c_1 V}. \tag{19}$$

3.1 Time Domain

Applying the Laplace and Fourier transform's defined by equations (12) and (13) on equations (8)-(11), we obtain

$$(\frac{d^2}{dx_2^2}-(\xi^2+p^2)d_1d_4)\tilde{u}_1-i\xi(d_2+d_3)\frac{d\tilde{u}_2}{dx_2}-(d_3-1)\frac{d\tilde{\phi}_3}{dx_2}+i\xi d_1d_4\tilde{T}=0\,, \tag{20}$$

$$-\frac{i\xi(d_2+d_3)}{d_4}\frac{d\tilde{u}_1}{dx_2}+(\frac{d^2}{dx_2^2}-\frac{\xi^2d_5}{d_4}-d_1p^2)\tilde{u}_2+\frac{i\xi(d_5-d_3)}{d_4}\tilde{\phi}_3-\bar{\beta}d_1\frac{d\tilde{T}}{dx_2}=0\,, \tag{21}$$

$$d_7(d_3-1)\frac{d\tilde{u}_1}{dx_2}-d_7i\xi(d_5-d_3)\tilde{u}_2+(\frac{d^2}{dx_2^2}-\xi^2d_6-d_7(d_5-2d_3+1)-d_8p^2)\tilde{\phi}_3=0\,, \tag{22}$$

$$-\frac{i\xi\varepsilon(p+n_0\tau_0p^2)}{K^*}\tilde{u}_1-\frac{\varepsilon\bar{\beta}(p+n_0\tau_0p^2)}{K^*}\frac{d\tilde{u}_2}{dx_2}+(\frac{d^2}{dx_2^2}-\frac{\xi^2+p+\tau_0p^2}{K^*})\tilde{T}=0\,. \tag{23}$$

Equations (20)-(23) after some algebraic calculation yield:

$$(\upsilon^8-A\upsilon^6+B\upsilon^4-C\upsilon^2+D)(\tilde{u}_1,\tilde{u}_2,\tilde{\phi}_3,\tilde{T})=0\,, \tag{24}$$

where

$$A=-f-a-a_{11}+\beta^{*2}g-h+b+d_7e^2\,,$$

$$B=f[a+a_{11}+h-b-d_7e^2]+g[-\beta^{*2}(a+h+d_7\varepsilon e^2)-\varepsilon\xi^2\beta^*(2d_2+d_3)]$$
$$+a(a_{11}+h-b)-a'+p^2hd_1-a_{11}d_7e^2-\frac{\xi ed_7(d_3-d_4)(d_5-d_3)}{d_4}\,,$$

$$C=f\{a_{11}d_7e^2+[-a_{11}-h+2b-2hd_1p^2-\xi^2(2d_2+d_3+d_4)]\}+g\{ah\beta^{*2}$$
$$+\xi^2a\varepsilon\beta^*(d_4-d_3)-2\beta^*\varepsilon\xi^2d_7e(d_5-d_3)+\varepsilon\xi^2d_4a_{11}\}+(a+h)a'\,,$$

$$D=(fh-\xi^2gd_4\varepsilon)(a_{11}a+a')\,,\qquad a=\xi^2d_6+d_7(d_5-2d_3+1)+d_8p^2\,,\qquad b=\xi^2\frac{(d_2+d_3)(d_2+d_4)}{d_4}\,,$$

$$e=d_3-1\,,\ f=\frac{\xi^2+p+\tau_0p^2}{K^*}\,,\ g=(1+\tau_1p)d_1(\frac{p+n_0\tau_0p^2}{K^*})\,,\ h=(\xi^2+p^2)d_1d_4\,,\ a_{11}=d_1p^2+\frac{\xi^2d_5}{d_4}\,,$$

$$a'=\frac{\xi^2d_7(d_5-d_3)^2}{d_4}\,,$$

and $\upsilon=\dfrac{d}{dx_2}$.

To solve this equation, we use Descarte's algorithm outlined below:

Shifting the roots of secular equation (24) by a factor of A/4 to eliminate the second term, we obtain

$$\zeta^4 + H\zeta^2 + G\zeta + I = 0. \tag{25}$$

where

$$\zeta = \upsilon - \frac{A}{4},\quad H = B - \frac{3A^2}{8},\quad G = \frac{AB}{2} - \frac{A^3}{8} - C,\quad I = D + \frac{A^2 B}{16} - \frac{2A^4}{256} - \frac{AC}{4}.$$

Factoring Equation (25) into two quadratic factors, we have

$$\zeta^4 + H\zeta^2 + G\zeta + I = (\varsigma^2 + l\varsigma + n)(\varsigma^2 - l\varsigma + n'). \tag{26}$$

Comparing the coefficients of various powers of ς in (26) on both sides, we get

$$n + n' = l^2 + H,\quad n - n' = \frac{G}{l},\quad nn' = I. \tag{27}$$

Eliminating n and n' from (27), we obtain

$$Z^3 + 2HZ^2 + (H^2 - 4I)Z - G^2 = 0, \tag{28}$$

where $Z = l^2$. Being cubic with complex coefficients, equation (28) can be solved by using the irreducible case of Cardon's method with the help of De Moivre's theorem. We again shift the roots of (28) by a factor of $\frac{-2H}{3}$ in order to obtain the standard cubic as

$$Y^3 - 3H^* Y - G^* = 0. \tag{29}$$

where

$$Y = Z + \frac{2H}{3},\quad H^* = \frac{(H^2 + 12I)}{9};\quad G^* = G^2 - \frac{8HI}{3} + \frac{2H^3}{27}. \tag{30}$$

Let the roots of equation (29) be of the type Y=U+V

so that

$$U^3 + V^3 = G^*,\quad U^3 V^3 = H^{*3}.$$

We may find the cube roots with the help of De Moivre's theorem, as shown below:

$$\text{Let} \quad U^3 = \frac{G^* + \sqrt{G^* - 4H^{*3}}}{2} = L + iM, \quad L, M \in R. \tag{31}$$

Then the values of U are given by

$$U_k = r^{\frac{1}{3}}(\cos\frac{2k\pi + \Phi}{3} + i\sin\frac{2k\pi + \Phi}{3}), \quad k = 0, 1, 2, \tag{32}$$

where $r = \sqrt{L^2 + M^2}$ and $\Phi = \tan^{-1}(\frac{M}{L})$. Having determined U, the values of V can be obtained from the relation $UV = H^*$ which further leads to the required values of Y and hence to the values of $l^2 = Z = Y - 2H/3$. One of the values of l so obtained is then used to evaluate m and n by equation (27). Using the values of m, n and l, the reduced secular equation (25) is factored into two quadratic factors of the type (26), which are further solved to obtain the four roots ς_i, $i = 1, 2, 3, 4$. The complex roots of secular equation (24) are obtained from the relation $\upsilon_i = \varsigma_i + A/4$, for $i = 1, 2, 3, 4$.

The solution of equation (24) satisfying the radiation condition that $\tilde{u}_1, \tilde{u}_2, \tilde{\phi}_3, \tilde{T} \to 0$ as $x_2 \to \infty$ is

$$(\tilde{u}_1, \tilde{u}_2, \tilde{\phi}_3, \tilde{T}) = \sum_{i=1}^{4} A_i (1, r_i, s_i, t_i) e^{-q_i x_2}, \tag{33}$$

where

$$r_i = \frac{a_1 q_i^5 + a_2 q_i^3 + a_3 q_i}{a_4 q_i^4 + a_5 q_i^2 + a_6}, \quad s_i = \frac{-a_1 q_i^3 + r_i (a_{10} q_i^2 - a_{11}) + a_9 q_i}{a_7 q_i^2 - a_8}, \quad a_1 = \frac{\beta^*}{i\xi d_4},$$

$$t_i = \frac{i\xi s_i q_i (d_3 - 1) - q_i^2 + h + i\xi r_i q_i (d_2 + d_3)}{i\xi d_1 d_4}, \quad a_2 = \frac{-\beta^* h + \xi^2 (d_2 + d_3) - a\beta^* + d_7 e^2}{i\xi d_4},$$

$$a_3 = \frac{a(\beta^* h - \xi^2 (d_2 + d_3) - \xi^2 d_7 e(d_5 - d_3))}{i\xi d_4}, \quad a_4 = 1 - \frac{\beta^* (d_2 + d_3)}{d_4}, \quad a_6 = aa_{11} - a',$$

$$a_5 = -a_{11} - aa_4 - \frac{\beta^* e(d_5 - d_3) d_7}{a'_4}, \quad a_7 = \frac{\beta^* e}{i\zeta a'_4}, \quad a_8 = \frac{i\xi (d_5 - d_3)}{a'_4}, \quad a_9 = \frac{\beta^* h - \xi^2 (d_2 + d_3)}{i\zeta a'_4}, \quad a_{10} = a_4.$$

Using equations (4), (6), (7) in the boundary conditions (14) and then applying Laplace and Fourier transforms defined by equations (12)-(13) with the help of (33), we get the transformed normal force stress, tangential force stress, tangential couple stress and temperature distribution as:

$$\tilde{t}_{22} = \frac{1}{\Delta}(\Delta_1 c_1^* e^{-q_1 x_2} + \Delta_2 c_2^* e^{-q_2 x_2} + \Delta_3 c_3^* e^{-q_3 x_2} + \Delta_4 c_4^* e^{-q_4 x_2})\bar{\eta}(p), \tag{34}$$

$$\tilde{t}_{21} = \frac{1}{\Delta}(\Delta_1 a_1^* e^{-q_1 x_2} + \Delta_2 a_2^* e^{-q_2 x_2} + \Delta_3 a_3^* e^{-q_3 x_2} + \Delta_4 a_4^* e^{-q_4 x_2})\bar{\eta}(p), \tag{35}$$

$$\tilde{m}_{23} = \frac{1}{\Delta}(\Delta_1 b_1^* e^{-q_1 x_2} + \Delta_2 b_2^* e^{-q_2 x_2} + \Delta_3 b_3^* e^{-q_3 x_2} + \Delta_4 b_4^* e^{-q_4 x_2})\bar{\eta}(p), \tag{36}$$

$$\tilde{T} = \frac{1}{\Delta}(\Delta_1 t_1 e^{-q_1 x_2} + \Delta_2 t_2 e^{-q_2 x_2} + \Delta_3 t_3 e^{-q_3 x_2} + \Delta_4 t_4 e^{-q_4 x_2})\bar{\eta}(p), \tag{37}$$

where

$$a_i^* = \frac{-d_3 i\xi r_i - q_i - e s_i}{d_1 d_4}, \quad b_i^* = \frac{q_i s_i}{d_1 d_4 d_7}, \quad c_i^* = \frac{-d_2 i\xi r_i - q_i r_i d_4 - \bar{\beta} t_i d_1 d_4}{d_1 d_4}, \ i = 1, 2, 3, 4.$$

$$\Delta = (c_1^* a_2^* - c_2^* a_1^*)(b_3^* s_4 - s_3 b_4^*) + (c_3^* a_1^* - c_1^* a_3^*)(b_2^* s_4 - s_2 b_4^*) + (c_1^* a_4^* - c_4^* a_1^*)(b_2^* s_3 - s_2 b_3^*) +$$
$$(c_2^* a_3^* - c_3^* a_2^*)(b_1^* s_4 - s_1 b_4^*) + (c_4^* a_2^* - c_2^* a_4^*)(b_1^* s_3 - s_1 b_3^*) + (c_3^* a_4^* - c_3^* a_4^*)(b_1^* s_2 - s_1 b_2^*),$$

$$\Delta_1 = -\tilde{P}_1\bar{\psi}_1(\xi)[a_1^*(b_3^* s_4 - s_3 b_4^*) - a_3^*(b_2^* s_4 - s_2 b_4^*) + a_4^*(b_2^* s_3 - s_2 b_3^*)] +$$
$$\tilde{P}_2\bar{\psi}_2(\xi)[c_2^*(b_3^* s_4 - s_3 b_4^*) - c_3^*(b_2^* s_4 - s_2 b_4^*) + c_4^*(b_2^* s_3 - s_2 b_3^*)],$$

$$\Delta_2 = \tilde{P}_1\bar{\psi}_1(\xi)[a_1^*(b_3^* s_4 - s_3 b_4^*) - a_3^*(b_1^* s_4 - s_1 b_4^*) + a_4^*(b_1^* s_3 - s_1 b_3^*)] -$$
$$\tilde{P}_2\bar{\psi}_2(\xi)[c_1^*(b_3^* s_4 - s_3 b_4^*) - c_3^*(b_1^* s_4 - s_1 b_4^*) + c_4^*(b_1^* s_3 - s_1 b_3^*)],$$

$$\Delta_3 = -\tilde{P}_1\bar{\psi}_1(\xi)[a_1^*(b_2^* s_4 - s_2 b_4^*) - a_2^*(b_1^* s_4 - s_1 b_4^*) + a_4^*(b_1^* s_2 - s_1 b_2^*)] +$$
$$\tilde{P}_2\bar{\psi}_2(\xi)[c_1^*(b_2^* s_4 - s_2 b_4^*) - c_2^*(b_1^* s_4 - s_1 b_4^*) + c_4^*(b_1^* s_2 - s_1 b_2^*)],$$

$$\Delta_4 = \tilde{P}_1\bar{\psi}_1(\xi)[a_1^*(b_2^* s_3 - s_2 b_3^*) - a_2^*(b_1^* s_3 - s_1 b_3^*) + a_3^*(b_1^* s_2 - s_1 b_2^*)] +$$
$$\tilde{P}_2\bar{\psi}_2(\xi)[-c_1^*(b_2^* s_3 - s_2 b_3^*) + c_2^*(b_1^* s_3 - s_1 b_3^*) - c_3^*(b_1^* s_2 - s_1 b_2^*)]. \tag{38}$$

In the time domain, boundary conditions defined by equation (14) must be used with

$$\eta(t) = \begin{cases} \delta(t) & \text{for Concentrated and Distibuted Force,} \\ H(t) & \text{for Moving Force.} \end{cases}$$

$$\bar{\eta}(p) = \begin{cases} 1 & \text{for Concentrated and Distributed Force,} \\ \dfrac{1}{p} & \text{for Moving Force.} \end{cases} \tag{39}$$

The expressions for stresses and temperature distribution in time domain can be obtained for Concentrated, Distributed and Moving Force by using the values of $\bar{\psi}_1(\xi), \bar{\psi}_2(\xi)$ from (15), (17) and (19) in equations (34)-(38) along with (39).

3.3 Frequency Domain

In this case, we assume time harmonic behavior as

$$(u_1, u_2, \phi_3, T)(x_1, x_2, t) = (u_1, u_2, \phi_3, T)(x_1, x_2)e^{i\omega t}, \tag{40}$$

In the frequency domain, boundary condition defined by equation (14) must be used with

$$\eta(t) = e^{i\omega t}. \tag{41}$$

The expressions for normal force stress, tangential force stress, tangential couple stress and temperature distribution in frequency domain can be obtained by replacing p with $i\omega$ and $\bar{\eta}(p)$ with $1/(p-i\omega)$ in the expressions of time domain.

3.4 Steady State

Following Fung /25/, the Galilean transformation

$$x_1^* = x_1 + U't, \; x_2^* = x_2, \; t^* = t, \tag{42}$$

is introduced, so that boundary conditions defined by equation (14) will take the form :

(i) $t_{22} = -P_1\psi_1(x_1^*)$,
(ii) $t_{21} = -P_2\psi_2(x_1^*)$,
(iii) $m_{23} = 0$,
(iv) T=0. (43)

In this case

$$\left.\begin{matrix}\psi_1(x_1^*)\\ \psi_2(x_1^*)\end{matrix}\right\} = \delta(x_1 + U't). \tag{44}$$

Using boundary conditions given by (43) with the help of (42) and (44) and following the same procedure as in the case of time domain, we can obtain the expressions for Normal force stress, Tangential force stress, Tangential couple stress and Temperature distribution in steady state by replacing p with $-ia\xi$ in the expressions of time domain, where $a = \dfrac{U'}{c_1}$.

3.5 Inclined Load

For an inclined load F_0, per unit length, we have

$$P_1 = F_0 \cos\theta \ , \quad P_2 = F_0 \sin\theta \, . \tag{45}$$

Using equation (45) in equations (34)-(38), we obtain the corresponding expressions for displacement and stress components in case of inclined load applied on the surface of the half space.

4 INVERSION OF THE TRANSFORM

The transformed stresses and temperature distribution are functions of x_2, the parameters of Laplace and Fourier transforms p and ξ, respectively, and hence are of the form $\bar{f}(\xi, x_2, p)$. To obtain the solution of the problem in the physical domain, we must invert the transform in (34)-(38) using

$$\bar{f}(x_1, x_2, p) = \frac{1}{2\pi} \int_{-\infty}^{\infty} \bar{f}(\xi, x_2, p) e^{-i\xi x_1} d\xi \ ,$$

$$\bar{f}(x_1, x_2, p) = \frac{1}{2\pi} \int_{-\infty}^{\infty} [\bar{f}_e \cos(\xi, x_2) - i\bar{f}_0 \sin(\xi, x_2)] d\xi \ , \tag{46}$$

where f_e and f_o are respectively even and odd parts of the function $\bar{f}(\xi, x_2, p)$. Thus, expressions (46) give us the transform $\bar{f}(\xi, x_2, p)$ of the function $f(x_1, x_2, t)$. Now, for the fixed values of ξ, x_1 and x_2, the function $\bar{f}(x_1, x_2, p)$ in the expression (46) can be considered as the Laplace transformed function $\bar{g}(p)$ of some function g(t). Following Honig and Hirdes /11/, the Laplace transformed function $\bar{g}(p)$ can be converted as given below.

The function g (t) can be obtained by using

$$g(t) = \frac{1}{2\pi i} \int_{c-i\infty}^{c+i\infty} e^{pt} \bar{g}(p) dp \ , \tag{47}$$

where c is an arbitrary real number greater than all the real parts of the singularities of $\bar{g}(p)$. Taking $p = c + ix_2$, we get

$$g(t) = \frac{e^{ct}}{2\pi i} \int_{-\infty}^{\infty} e^{itx_2} \bar{g}(c + ix_2) dx_2 \ . \tag{48}$$

Now, taking $e^{-ct}g(t)$ as h (t) and expanding it as Fourier series in [0,2L], we obtain approximately the formula

$$g(t) = g_\infty(t) + E'_D,$$

where

$$g_\infty(t) = \frac{c_0}{2} + \sum_{k=1}^{\infty} c_k \ , \ 0 \le t \le 2L \ , \ c_k = \frac{e^{ct}}{L}\Re[e^{\frac{ik\pi t}{L}}\bar{g}(c+\frac{ik\pi}{L})], \tag{49}$$

E_D is the discretization error and can be made arbitrarily small by choosing c large enough .The value of c and L are chosen according to the criteria outlined by Honig and Hirdes /11/.

Since the infinite series in equation (48) can be summed up only to a finite number of N terms, the approximate value of g(t) becomes

$$g_N(t) = \frac{c_0}{2} + \sum_{k=1}^{N} c_k \ , \ 0 < t < 2L \, . \tag{50}$$

Now, we introduce a truncation error E_T that must be added to the discretization error to produce the total approximation error in evaluating g(t) using the above formula. Two methods are used to reduce total error. The discretization error is reduced by using the 'Korrecktur' method, Honig and Hirdes /11/ and then ε-algorithm' /25,26/ is used to reduce the truncation error and hence to accelerate the convergence.

The 'Korrecktur' method formula, to evaluate the function g(t) is

$$g(t) = g_\infty(t) - e^{-2cL}g_\infty(2L+t) + E_{D'}$$

where $|E'_D| << |E_D|$. Thus the approximate value of g(t) becomes

$$g_{N_k}(t) = g_N(t) - e^{-2cL}g_{N'}(2L+t), \tag{51}$$

where N' is an integer such that $N' < N$.

We shall now describe the ε-algorithm which is used to accelerate the convergence of the series in equation (49). Let N be a natural number and $S_m = \sum_{k=1}^{m} c_k$ be the sequence of partial sums of equation (49). We define the ε-sequence by

$$\varepsilon_{0,m} - 0\ ,\ \varepsilon_{1,m} - S_m\ ,\ \varepsilon_{n+1,m} - \varepsilon_{n-1,m+1} + \frac{1}{\varepsilon_{n,m+1} - \varepsilon_{n,m}}\ ,\ \text{n,m,-1,2,3,.....}$$

It can be shown by Honig and Hirdes /11/ that the sequence $\varepsilon_{1,1}, \varepsilon_{3,1}, \ldots\ldots\ldots\ldots \varepsilon_{N,1}$ converges to $g(t) + E_D - \frac{c_0}{2}$ faster than the sequence of partial S_m, m=1,2,3..... The actual procedure to invert the Laplace Transform reduces to the study of equation (50) together with an ε-algorithm.

The last step in the inversion process is to evaluate the integral (46). This has been done using Romberg's integration with adaptive size. This method uses the results from successive refinements of the extended trapezoidal rule followed by extrapolation of the results to the limit when the step size tends to zero. The details can be found in /29/.

5. NUMERICAL RESULTS AND DISCUSSIONS:

For numerical computations, we take the non dimensional values for orthotropic micropolar thermoelastic solid with one relaxation time as,

$d_1 = 1.02$, $d_2 = 0.7888$, $d_3 = 1.9828$, $d_4 = 6.0224$, $d_5 = 1.32$, $d_6 = 1.53$, $d_7 = .00104$, $d_8 = 1.6543$.

Following Gauthier /10/ we take, the non dimensional values for Aluminium Epoxy like composite as

$d_1 = 1$, $d_2 = 0.667$, $d_3 = .992$, $d_4 = 5.977$, $d_5 = 1$, $d_6 = 1$, $d_7 = .001167$, $d_8 = .847$.

The comparison of normal force stress, tangential couple stress and temperature distribution for orthotropic micropolar thermoelastic solid with one relaxation time (OMST) and isotropic micropolar generalized thermoelastic solid (IMST) have been shown in Figures 1-21. The computations were carried out at x_2=0.1 within the range $0 < r_i < 10$. The curves represented by solid line with or without centre symbol correspond to the case of MOS whereas the curves represented by dotted lines with or without centre symbol correspond to the case of MIS. All the results are shown for one value of dimensionless width $a_0 = \frac{\omega^* a}{c_1} = 1$ and three values of dimensionless speed $V_0 = \frac{V}{c_1} = 5,\ 10,\ 15$. In Figures 1-18 solid and dotted line without center symbol represents the variations for $\theta = 0^0$ (initial angle), solid and dotted lines with center symbol $(-0-0-)$ represent the variations for $\theta = 45^0$ (intermediate angle) and solid and dotted line with center symbol $(-\times-\times-)$ represents the variations for $\theta = 90^0$ (extreme angle). In Figures 19-21 solid and dotted

lines without center symbol represent the variations for dimensionless speed V=5, whereas solid and dotted line with center symbol (–0–0–) represent the variations for dimensionless speed V=10, and solid and dotted line with center symbol (–×–×–) represent the variations for dimensionless speed V=15.

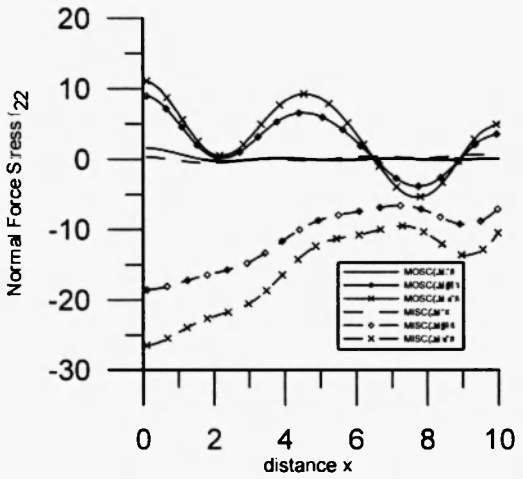

Fig. 1: Variation of t_{22} with distance x due to concentrated source in time domain

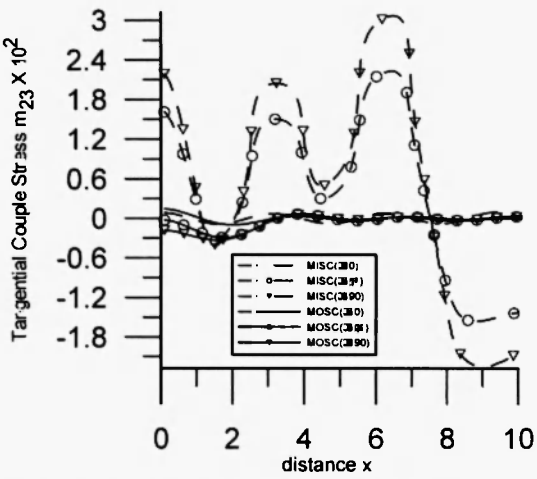

Fig. 2: Variation of m_{23} with distance x due to concentrated source in time domain

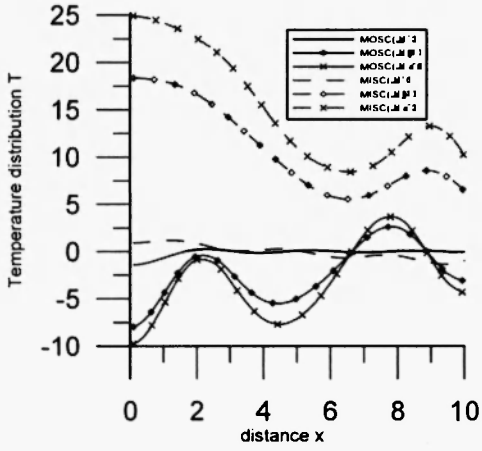

Fig. 3: Variation of T with distance x due to concentrated source in time domain

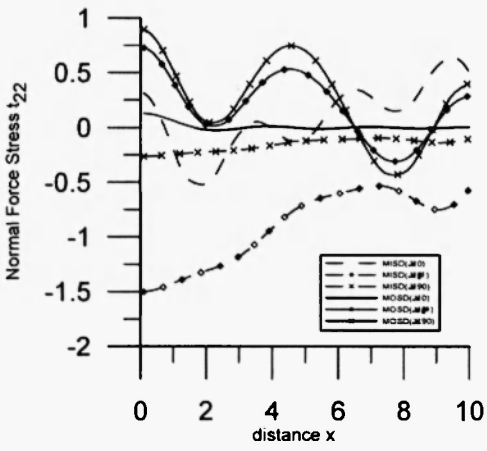

Fig. 4: Variations of t_{22} with distance x due to distributed source in time domain

5.1 Concentrated Force

Figures 1-3, 7-9, 13-15 depict the variations due to concentrated force.

5.1.1 Time Domain

Figure1 shows the variations of normal force stress t_{22} with distance x. The values of normal force stress t_{22}, at initial angle of inclination initially decreases then attains a constant value for both MOS and MIS and as the angle of inclination increases (θ = 45°, 90°) for MOS its values oscillate an simultaneously deceases with an increase in x, whereas for MIS its values increase with an increase in distance x. The values of t_{22} are greater for MOS as compared to that of MIS.

It is evident from Figure 2 that for MOS the values of tangential couple stress m_{23} initially deceases then increases and then oscillates with very small magnitude for all values of θ. However for MIS and at initial inclination angle and for MIS, it has same variations as that of MOS, while for remaining angles its value oscillates with increasing magnitude. In this case the values for MOS are less as compared to that of MIS.

Figure 3 shows the variations of temperature distribution T with distance x. The values of T for MOS and when θ = 45°, 90° oscillates with increasing magnitude, while for MIS exactly the opposite behavior is observed. At initial angle of inclination its value starts with initial increase and then tends to attain a constant value for both MIS and MOS.

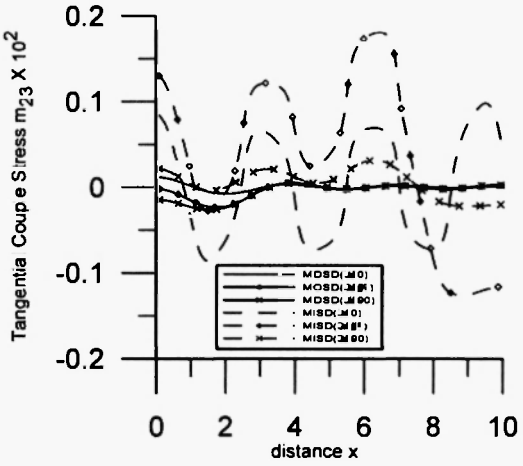

Fig. 5: Variation of m_{23} with distance x due to distributed source in time domain.

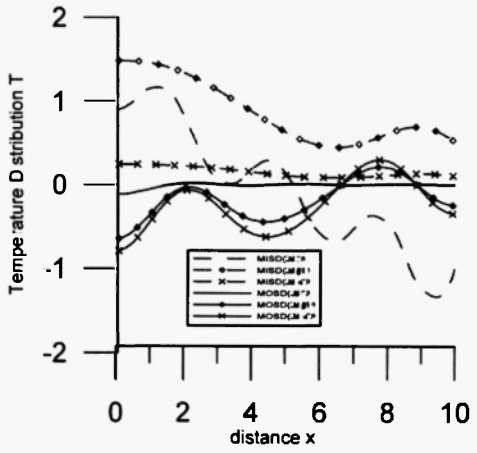

Fig. 6: Variations of T with distance x due to distributed source in time domain.

5.1.2 Frequency Domain

Figures 7-9 shows the variations with distance x in frequency domain. It is observed from Figure 7 that for MOS and at intermediate and extreme angle, the values of t_{22} start with small initial increase then decrease sharply in the range $1 < x < 4.5$; with further increase in distance x its value oscillates with decreasing magnitude, while for MIS its values start with sharp initial increase in the range $0 < x < 2$ then alternately increase and decrease with distance x. When $\theta = 0^0$ and for both MOS, MIS its values are distributed in large range but with very small magnitude. The values of t_{22} for MOS are smaller than those of MIS.

Figure8 shows the variations of m_{23} with distance x. For MOS and at $\theta = 45°, 90°$ its values oscillate with very small magnitude. However at intermediate angle its value alternately increases or decreases with increase in distance x whereas for MIS its behavior is opposite as compared to that of MOS. The values of m_{23} for MIS and when $\theta = 45°, 90°$ have been shown in the figure by multiplying its original value by 100.

It is observed from Figure 9 that the value of T for both MOS and MIS when $\theta = 0°$ oscillates in very large range but with very small magnitude. While when $\theta = 45°, 90°$ for MOS its value starts with initial decrease and then increases sharply in the range $1 < x < 5$; after that its value alternately increases or decreases with further increase in distance x. However for MIS and both intermediate and extreme angle of inclination its values start with sharp decrease and then oscillates with increase in distance x.

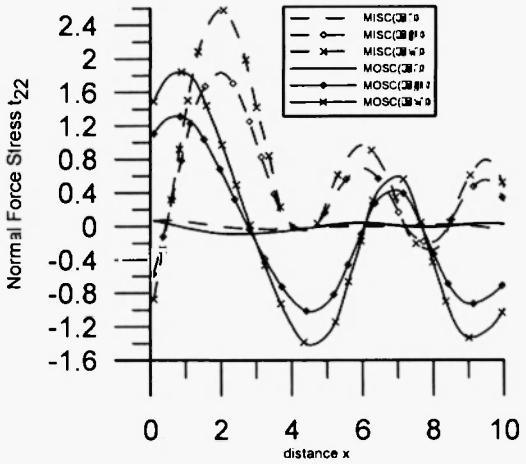

Fig. 7: Variation of t_{22} with distance x due to concentrated source in frequency domain.

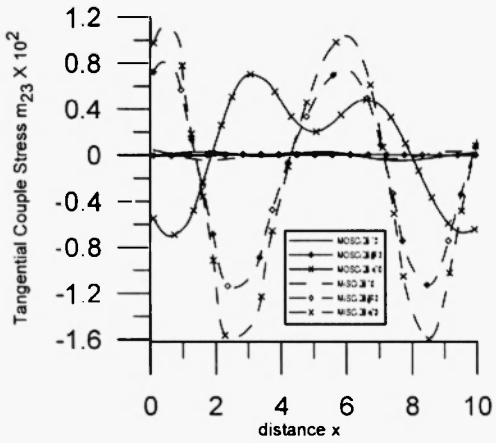

Fig. 8: Variations of m_{23} with distance x due to concentrated source in frequency domain.

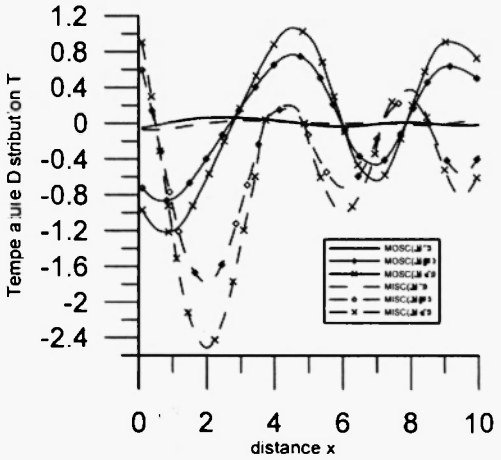

Fig. 9: Variation of T with distance x due to concentrated source in frequency domain

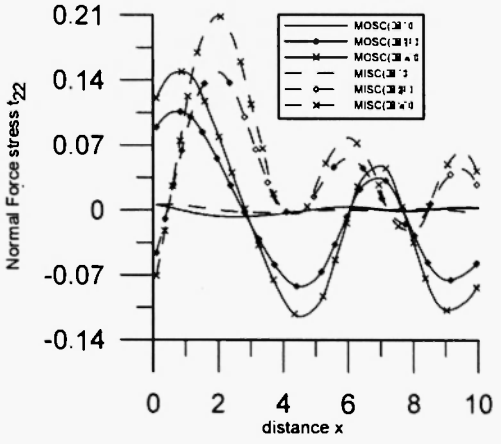

Fig. 10: Variation of t_{22} with distance x due to distributed source in frequency domain.

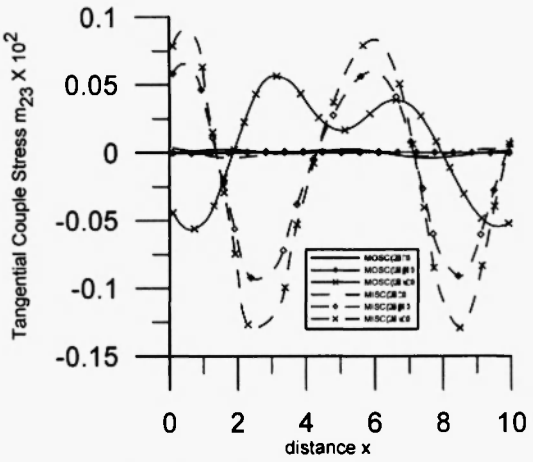

Fig. 11: Variation of m_{23} with distance x due to distributed source in frequency domain

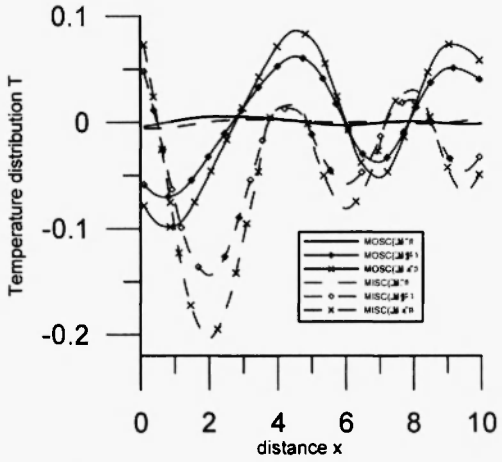

Fig. 12: Variation of T with distance x due to distributed source in frequency domain

5.1.3 Steady State

Figures13-15 show the variations with distance x in steady state. In Figure 13 it is observed that for both MOS and MIS and all values of θ, the value of t_{22} oscillates with decreasing magnitude.

Figure14 shows that at an initial angle of inclination for MOS the values of m_{23} initially increase then decreases with increase in x, while for MIS its values oscillate with small magnitude. At intermediate angle of inclination its values initially increases and then decreases with increase in distance x for both MOS and MIS .While at extreme inclination for MOS its values initially decreases and then increases sharply in the range $0.2 \leq x \leq 4$ and then remains constant for remaining value of x, while for MIS its values oscillates with increase in x.

Figure 15 shows that for MOS and intermediate and extreme angle of inclination the value of T initially decreases, then oscillates with increasing magnitude and at an initial angle it oscillates with increasing magnitude, while for MIS and all angles of inclination its value initially increases and then decreases with distance x.

5.2 Distributed Force

5.2.1 Time Domain

Figure 4 shows that for MOS when $\theta = 45°, 90°$ the value of t_{22} oscillates with decreasing magnitude with increase in distance x, while for MIS its values increases with increase in distance x. However for MOS and for initial angle of inclination its value initially decreases then appears to be steady for all values of x, while for MIS its value oscillates with increasing magnitude.

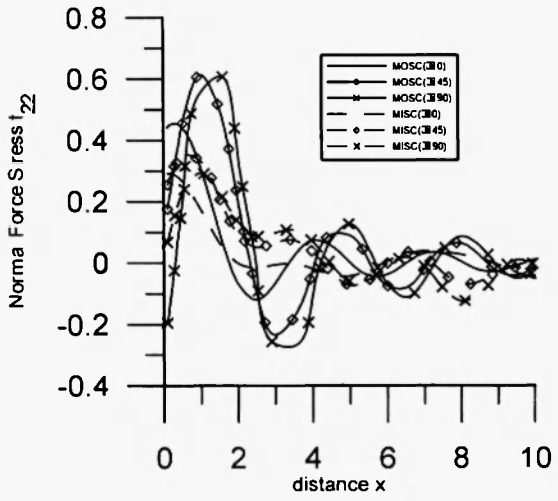

Fig. 13: Variation of t_{22} with distance x due to concentrated source

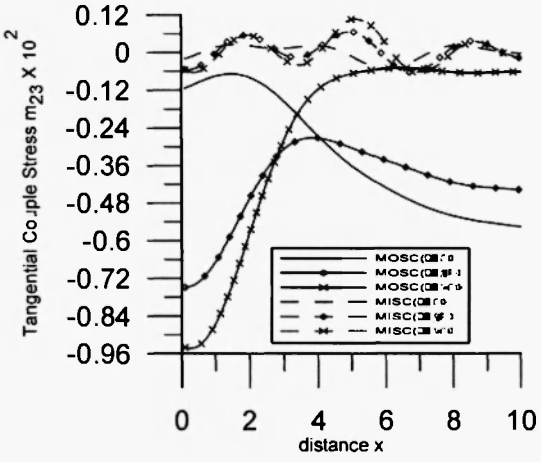

Fig. 14: Variation of m_{23} with distance x due to concentrated source

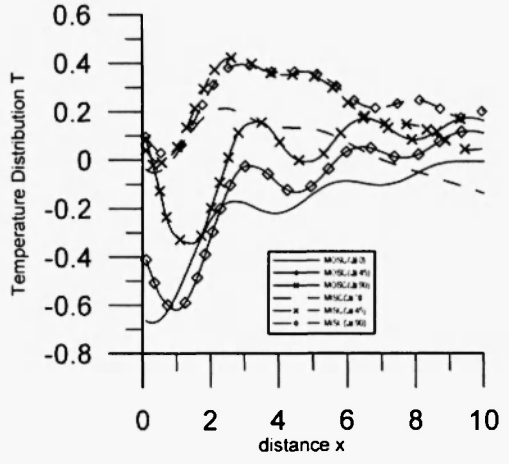

Fig. 15: Variation of T with distance x due to concentrated source

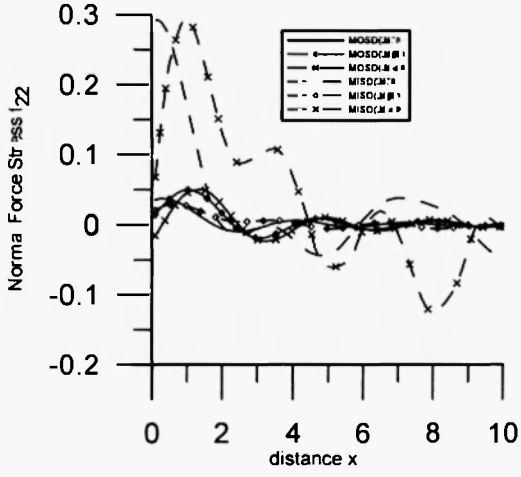

Fig. 16: Variation of t_{22} with distance x due to distributed source

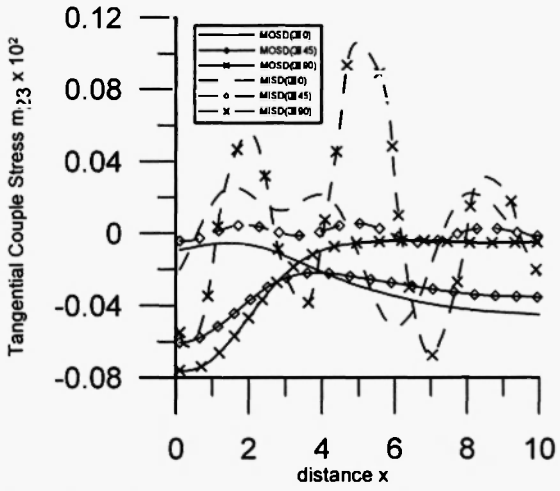

Fig. 17: Variation of m_{23} with distance x due to distributed source

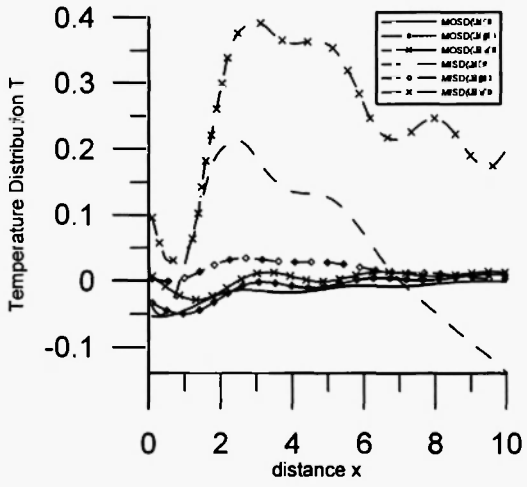

Fig. 18: Variation of T with distance x due to distributed source

Figure 5 shows that the values of m_{23} for MOS and at all angles initially decrease and then attain a constant value with increase in x, while for MIS its values initially decrease and then oscillate with large magnitude.

Figure 6 shows the variations of temperature distribution T with distance x. The value of T for MOS and when $\theta = 45°, 90°$ oscillates with increasing magnitude, while for MIS its values decrease with increase in x. When $\theta = 0°$ and for MOS its values start with initial increase and then attain a constant value, while for MIS its values oscillate with decreasing magnitude.

5.2.2 Frequency Domain

Figs 10-12 show the variations of normal force stress, tangential couple stress and temperature distribution in frequency domain. In this case the values of normal force stress, tangential couple stress and temperature distribution vary in a similar way to that of concentrated force but with difference in magnitude.

5.2.3 Steady State

Figures 16-18 depict the variations due to distributed force in the case of steady state. From Figure 16 it is observed that, as we fix the point of observation, i.e., the value of distance 'x', the normal displacement t_{22} for MOS increases or decreases with change in angle of inclination. With further increase in inclination angle, it is revealed that stress follows an oscillatory pattern about zero value, ultimately becoming zero, while for MIS its value oscillates with decreasing magnitude with change in distance 'x'.

Figure 17 shows that for MOS and at initial and intermediate angle of inclination the values of m_{23} initially increases and then decreases with further increase in x, while when $\theta = 90°$ its values increase with increase in x. For MIS the magnitude of m_{23} increases or decreases along an oscillatory path with increase in

distance x. It is revealed that with an increase in distance each curve follows an oscillatory pattern.

It is observed from Figure 18 that the value of 'T' in the case of MOS increases or decreases with an angle of inclination, with further increase in inclination it is observed that T follows an oscillatory pattern about zero value which becomes zero ultimately. For MIS and all values of θ, the values of T initially decrease and then increase sharply in the range $1 < x < 3$, then decrease with further increase in x.

5.3 Moving Force

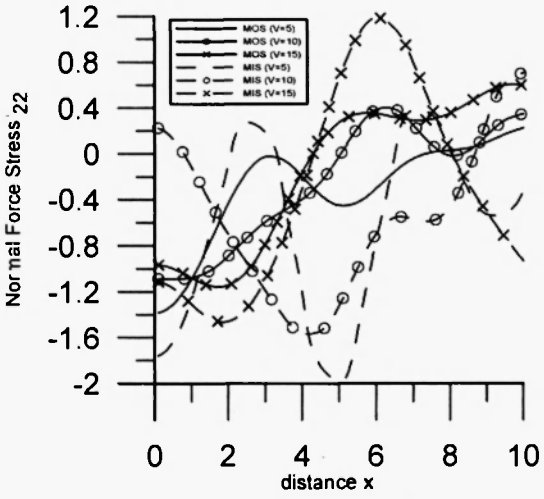

Fig. 19: Variation of t_{22} with distance x due to moving source in time domain

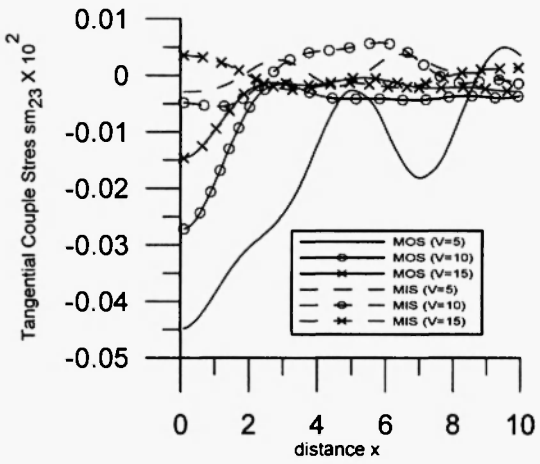

Fig. 20: Variation of m_{23} with distance x due to moving source in time domain

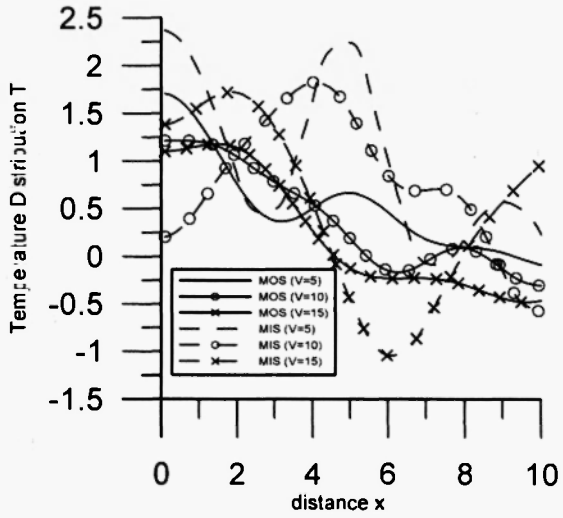

Fig. 21: Variation of T with distance x due to moving source in time domain

Figures 19-21 depict the variations of t_{22}, m_{23}, T due to the moving force in the time domain. It is observed from Figure 19 that for MOS the maximum (absolute) normal stress t_{22} occurs corresponding to the maximum velocity (V=15), i.e., impact of moving force is larger for large velocities. Further it is observed that for MIS, when V=10, 15 the value of t_{22} initially decreases and then increases with further increase in x, while it oscillates with large magnitude for V=5.

Figure 20 shows that the values of m_{23} for MOS and for all values of V initially increase and then oscillates with increase in x. However its behavior is opposite in nature for MIS when V=10,15 but the same for V=5 as compared to that of MOS. The values of m_{23} for MIT have been shown in the figure by dividing its original value by 100.

It is observed from Figure 21 that the variations in the values of T are opposite to that of t_{22} .

6. OBSERVATIONS

It is observed from the above discussion that, due to the effect of anisotropy, the values of normal force stress t_{22} are increased with the application of both concentrated and distributed source, while its value decreased when moving source is applied. However the values of tangential couple stress m_{23} and temperature distribution T get decreased with increase in anisotropy. A significant effect of change in angle of inclination is also observed on the values of t_{22} , m_{23} and T. On the application of concentrated source, as the angle of inclination increases, the value of t_{22} increases while that of m_{23} and T decreases. Similar behavior is observed on the application of distributed and moving sources. In frequency domain, the values of t_{22} and m_{23} are decreased with increase in anisotropy while reverse behavior is observed in the values of temperature distribution T. Also, as the angle of inclination increases, the values of t_{22} are increased while reverse behavior is observed in the values of m_{23} and T. For steady state, anisotropy tend to increase the value of normal force stress t_{22} whereas the values of m_{23} and T are decreased. With increase in the angle of inclination the value of t_{22} and T is increased for both MOS and MIS, whereas exactly opposite behavior is observed in the values of m_{23}.

7. REFERENCES

1. Chandershekharia, D.S, 1986, Heat flux dependent micropolar thermoelasticity. *International Journal of Engineering Science*, **24**, 1389-1395.
2. Iesan, D., 1974, On the positive definiteness of the operator of micro polar elasticity, *J. Engg. Math.*, **8**,107-112.
3. Dost, S.,and Tabarrak, B.,1978, Generalized micropolar thermoelasticity *International Journal of*

Engineering Science,**16**,173-183.

4. Eringen A.C, 1968, Theory of micropolar elasticity. In: *Fracture*, H. Liebowitz (Ed.), Vol. II. Academic Press, New York.
5. Eringen A.C., 1970, Foundations of micropolar thermoelasticity. Course of lectures No.**23**,CSIM Udine Springer.
6. Eringen A.C., 1992, Balance laws of micromorphic continua. I. *International Journal of Engineering Science*, **30**, 805-810.
7. Eringen A.C., 1999, *Microcontinum Field Theories. I. Foundations and Solids*, Springer-Verlag,New York.
8. Eringen A.C., 2001, *Microcontinum Field Theories. II. Fluent Media*, Springer-Verlag, New York.
9. Maugin, G.A.and Mild, 1986, A. Solitary waves in micropolar elastic crystals. *International Journal of Engineering Science*, **24**, 1477-1499.
10. Gauthier R.D., 1982, In: *Experimental investigations on micropolar media, Mechanics of Micropolar Media.* O. Brulin and RKT Hsieh (Eds). (Singapore: World Scientific).
11. Honig, G., Hirdes, V., 1984, A method for the numerical inversion of the Laplace transform, *J.Comput.Appl.Math.* **10**, 113-132.
12. Janusz Dyszlewicz, 2003, Micropolar Theory of Elasticity, Lecture notes in applied and computational mechanics.
13. Nowacki, W., 1966, Couple stress in the theory of thermoelasticity. *Proc.ITUAM Symposia*, Vienna, H. Parkus and L.I. Sedov (Eds.), Springer-Verlag, 259-278.
14. R. Kumar, P. Aliwalia, 2005, Electrodynamics of inclined loads in a micropolar cubic crystal, *Mech. and Mechanical Engg.*, 9(2), 57-75.
15. R. Kumar, P. Aliwalia, 2005, Moving inclined load at boundary surface, *Appl.Math. and Mech.* (English Edition), **26**(4), 476-485.
16. R. Kumar, P. Aliwalia, 2005, Interactions due to inclined load at micropolar elastic half-space with voids, *IJAME*, **10**(1), 109-122.
17. R. Kumar, L. Rani, 2005, Response of thermoelastic half-space with voids due to inclined load, *IJAME*, **10**(2), 281-294.
18. R. Kumar, L. Rani, 2005, Deformation due to inclined load in thermoelastic half space with voids, *Arch.Mech*, **57**(1), 7-24.
19. R. Kumar, S. Choudhary, 2003, Response of orthotropic micropolar medium under the influence of various sources, *Mechanica* **38**,349-368.
20. R. Kumar and S. Choudhary, 2004, Dynamical behavior of orthotropic micropolar elastic medium, *J.Vibration.Control.* **8**:1053-1069.
21. R. Kumar and P. Ailawalia, 2004, Effects of fluid layer at micropolar orthotropic boundary surface.,"*Sadhana*" Part 6, **29**, 605-616.

22. R. Kumar and P. Ailawalia, 2006, Interactions due to mechanical sources in micopolar cubic crystal, *IJAME*, **11**(2),337-357.
23. R. Kumar and P. Ailawalia, 2006b, Deformation due to time harmonic sources in micropolar thermoelastic medium possessing cubic symmetry with two relaxation times, *Applied Mathematics and Mechanics* (English Edition) **27**(6), 781-792.
24. R. Kumar and P. Ailawalia, 2007, Deformation due to moving load at boundary surface, *Science and Engineering of Composite Materials*, **14**, 25-46.
25. K.S. Crump, 1976, Numerical inversion of Laplace transforms using a Fourier series approximation, *J. ACM*, **23**(1), 89-96.
26. F. Vellion, Quelques methods nouvelles pour le calcul numerique de la transformer inverse de Laplace, Th. Univ. de Grenoble, 1972.
27. R.S. Dhaliwal and A. Singh,1987, Micropolar thermoelasticity, in: *Thermal Stresses II, Mechanical and Mathematical Methods*, Ser.2, R. Hetnarski (Ed.), North-Holland.
28. T.R. Tauchert, W.D. Claus, and T. Ariman, 1968, The linear theory of micropolar thermoelasticity, *International Journal of Engineering Science*, 637-47.
29. W.H. Press, S.A. Teukolshy, W.T. Vellering and B.P. Flannery, 1986, *Numerical Recipes*, Cambridge University Press, Cambridge.
30. Y.C. Fung, 1968, *Foundations of Solid Mechanics* [M], Prentice Hall, New Delhi.